Received: 13 June 2022 | Revised: 21 August 2022 | Accepted: 22 August 2022 | Published on: 11 September 2022

DOI: 10.1002/ctpp.202200092

ORIGINAL ARTICLE

Contributions to Plasma Physics

Shockwave and spallation in silver and other materials by sub-ns laser pulse at 10^{16} W/cm^2 intensity

Lorenzo Torrisi[1,2] | **Alfio Torrisi**[3,4]

[1]Department of Mathematical and Computer Sciences, Physical Sciences and Earth Sciences, MIFT, University of Messina, Messina, Italy

[2]INFN-Sections of Catania, Catania, Italy

[3]Department of Mathematics and Physics "E. De Giorgi", University of Salento, Lecce, Italy

[4]INFN-Section of Lecce, Lecce, Italy

Correspondence
Lorenzo Torrisi, Department of Mathematical and Computer Sciences, Physical Sciences and Earth Sciences, MIFT, University of Messina, V. le F.S. d'Alcontres 31, 98158 S. Agata, Messina, Italy.
Email: lorenzo.torrisi@unime.it

Abstract

The laser spallation effect due to intense shockwaves caused by a brief and intense laser pulse irradiating a target surface, 2 mm thick, has been investigated for silver and other materials. For 300 ps IR laser pulse, at intensities of the order of 10^{16} W/cm^2, the shockwave may produce deformations of the back-face in ductile materials, such as Ag, Cu and Al. In heavy materials with high tensile strength, such as Ta, the shockwave produces cracks in the bottom of the laser crater but not deformation in the back-face, while in brittle materials, such as monocrystalline Ge, it produces only superficial cracks and flaking, but not deformation and spallation of the back-face. In thick polymeric materials, such as high-density polyethylene, the ablated crater shape is well defined and the shockwave is strongly damped, and no deformation has been observed in the back-face. The laser ablation yield and the ion acceleration in the backward direction have been measured by mass lost and time-of-flight measurements. SEM microscopy of the different irradiated targets, showing details of the crater size, edges, flaking and deformation in the back-face, useful for a discussion on the shockwave propagation and shock pressure calculation, is presented.

KEYWORDS

crater, laser ablation, laser shockwave, laser spallation, Mach number, shockwave velocity

1 | INTRODUCTION

Laser-induced spallation is a process in which a stress wave generated from a rapid, high-energy laser pulse deposition initiates the ejection of surface material opposite to the surface of laser impingement.[1] Laser spallation is a phenomenon extensively studied in ballistic field, due to the shockwave of a laser pulse focused on a material and causing its fracture or deformation. The term spall is used in laser shockwave research when a wave front hits orthogonally a material surface, producing a dynamical tension perpendicular to this plane.[2] The evolution of laser spallation begins with the generation of shockwaves produced by laser vaporization of the target surface and develops as a confinement of plasma at the solid–vacuum surface producing a stress on the order of gigapascals (GPa) or higher, proportionally to the used laser energy.[3] When the amplitude and duration of this shockwave is enough, spallation will occur near the surface of the target sheet. Thus, a high intensity laser pulse is utilized to create a high-amplitude compressive stress pulse in the target. The compressive stress pulse propagates through the substrate and then reflects as a tensile wave at the free

boundary with enough magnitude to cause deformation of a monolithic material surface.[1,4] It can be used to enhance the target density, to produce interface adhesion, to cleaning surfaces, to stress interfaces and covering film measuring their mechanical resistance and others.[1,5,6]

The shockwave pulse reflection from the rear surface of a sheet target produces the appearance of a rarefaction wave into the target. This effect causes a tension within the target due to the crossing of two opposite rarefaction waves, the first coming from the front surface produced by the fall of the input pressure, and the second coming from the rear surface reflected wave.[1,7] In conditions of high magnitude and duration, this tension is enough to produce an internal rupture, called spall.

In ductile materials, the spall effect is localized by plastic deformation around small voids that grow and coalesce to form the spall plane.[8]

Using high laser intensity, higher than 10^{12} W/cm^2, and sub-ns laser pulses, very high tensions can be induced into the target. The radiation pressure, due to the exchange of momentum between the target and the electromagnetic field, is calculated using the Poynting vector, S, from the following equation[9]:

$$P = S/c = I/c \qquad \text{(Pa)}, \tag{1}$$

where c is the light velocity and I is the laser intensity (W/m^2). Equation (1) is valid for a black body (full absorbent), while in the case of a perfect reflector, the reflected wave will further contribute to the radiation pressure giving:

$$P = 2\,I/c. \tag{2}$$

Thus, the maximum radiation pressure for a laser intensity of 10^{16} W/cm^2 hitting a reflecting target (plasma) is:

$$P = 2\,I/c = \left(2 \times 10^{16}\ \text{W}/10^{-4}\ \text{m}^2\right) / \left(3 \times 10^{8}\ \text{m/s}\right) = 6.7 \times 10^{11}\ \text{Pa} = 670\ \text{GPa} \tag{3}$$

which may cause material rupture and cracks because, generally, it is above the tensile strength of many materials.

The literature reports that metals can be broken by laser shots because the shockwave pressure exceeds their breaking load. At low laser intensity irradiating aluminium target values of 167 MPa for 4.3 J/cm^2 fluence and 13 ns pulse duration have been measured,[10] at medium intensity (10^{13} W/cm^2) in different metals (Al, Fe, Ta, Au) the pressure may reach values of about 400 GPa[11] and at high laser intensity values of about 10^{15} Pa using an intensity of 10^{17} W/cm^2, 80 mJ pulse energy and 30 fs pulse duration can be achieved.[12]

The high intensity laser ablation of thick materials generally produces a crater, inside which the plasma is confined by the crater walls. The hydrodynamic expansion of the heated plasma in the confined region creates the high-amplitude short-duration pressure pulse and a shock process.

Efficient absorption of laser energy in the plasma is required to create the intense pressure pulses and shockwave. Energy losses due to reflections from the surface and absorption in a surrounding gas environment or plasma plume formed by the laser vaporized material will reduce the maximum shock pressures which can be generated.

At the used high laser intensity, the laser–matter interaction may induce high deformation in ductile materials and dynamic crack propagation in brittle materials, which can break and explode, as in metals and glasses.[13] Instead, their effect in many polymers may be strongly damped, the pressure wave, in fact, decreases exponentially with the distance; here the crater shape of the ablated material may be well defined and free from cracks induced by the impact laser shockwave pressure and cavitation and molecular fragmentation effects may occur.[14]

The strain ε produced by plastic deformation of a ductile material is defined as $\Delta l/l$, where Δl is the difference between the final and original lengths of the target in one dimension and l is the original length. In three dimensions, the strain is defined as $\Delta V/V$, that is, as the relative change in the volume. One important parameter described in the spall creation is the strain rate, ε_r, defined as:

$$\varepsilon_r = d\varepsilon/\text{dt}. \tag{4}$$

The literature reports that high-power shot-pulse lasers have been used to generate strain rates higher than 5×10^8 s^{-1}.[1,4]

One aim of this paper is to evaluate the strain rate in Ag and other targets using a sub-ns IR laser operating at about 10^{16} W/cm^2 intensity.

Using unfocused laser beams and thin targets, in which the spot diameter is higher than the target thickness, the shockwave is planar, while using focused laser beam and thick targets, in which the spot size is smaller to the target thickness, the shockwave is spherical.[4,13]

The main parameters to be calculated to investigate the spall effect, due to spherical shockwaves induced by focused laser pulses in thick targets, according to the literature, are[15]:

1. The shockwave radius r_s depending on the time, t, pulse laser energy E and density of the undisturbed material ρ:

$$r_s(t) = t^{2/5}(E/\rho)^{1/5}\, Y(\gamma), \tag{5}$$

where $Y(\gamma)$ is an empirical constant depending on the gas adiabatic constant γ, which generally assumes values within 0.9 and 1.15, according to the literature.

2. The expansion velocity of the shockwave, v_s, depends on the following parameters:

$$v_s(t) = \frac{dr_s}{dt} = \frac{2}{5}\, t^{-3/5}(E/\rho)^{1/5}\, Y(\gamma). \tag{6}$$

3. The Mach number of the shockwave M_s, calculated with respect to the sound velocity in the undisturbed medium at T temperature, $u(T)$ is:

$$M_s(t) = \frac{v_s(t)}{u\,(T)}. \tag{7}$$

4. The pressure jump, Δp, across the shockwave according to the literature[15] can be calculated as follows:

$$\Delta p = \frac{8}{25}\left(\frac{1}{\gamma+1}\right)\left(\frac{E}{r_s^3}\right) Y^5(\gamma). \tag{8}$$

Equation (8) is only valid in the near field, where the shockwave travels with a velocity well above the speed of sound, while in the far field the shockwave slows down, and begins to behave as a sound wave.

2 | MATERIALS AND METHODS

The investigations were performed at the PALS research laboratory in Prague with the use of an iodine laser operating at 1315 nm, 300 ps pulse duration, with a maximum pulse energy of about 600 J.[16] The laser beam was focused on the flat surface of a target placed in a vacuum chamber at 10^{-6} mbar. The focal position of the convergent lens was placed at the target surface, at which a focus spot of 100 μm diameter is created. The incidence angle of the laser beam on the target was 15°. The laser pulse energy was changed from about 25 J up to about 600 J. The maximum laser intensity was 2.55×10^{16} W/cm^2. Laser was employed in a single shot.

The used targets were 1.5 cm × 2 cm sheets with 2 mm thickness of polyethylene (PE), Al, Cu, Ge (monocrystalline), Ag and Ta with polished and flat surface. The polymer is UHMWPE (ultra-high molecular weight polyethylene) type, with a density of 0.97 g/cm^3 and with monomer stoichiometry $(CH_2)_n$.

Ion collectors (IC) and SiC detectors were used in time-of-flight (TOF) technique in order to measure the maximum ion energies for light at heavy ions and to evaluate the maximum charge state along the normal direction to the target surface and for angles close to this direction (±15°). Both detector types are connected through a low capacitance to a fast storage oscilloscope (Tektronix, 20 GS/s) to acquire their temporal signals indicating the X-ray photopeak at the start time, the electron detection and, successively, the fast and slow ion detection, as presented in our previous papers.[17,18]

Their flight length is generally higher than 1 m, as will be given for each TOF spectrum.

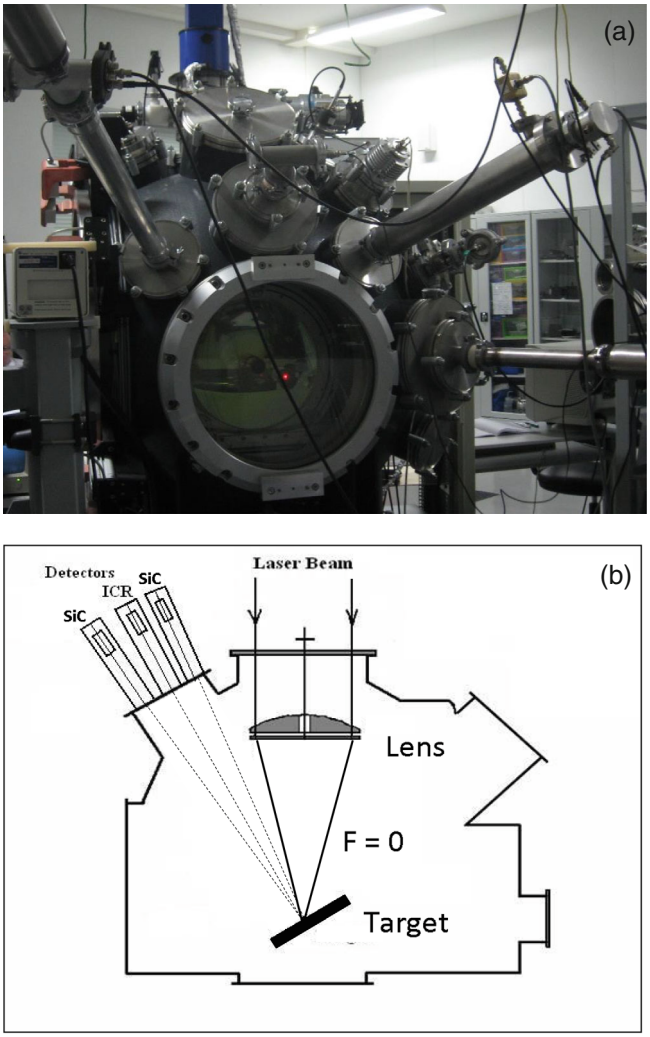

FIGURE 1 Photo (a) and scheme (b) of the employed set-up at PALS

A photo and a scheme of the experimental apparatus are reported in Figure 1a,b, respectively.

The electronic and nuclear ion energy loss, range, straggling and sputtering yield have been calculated using the SRIM code.[19]

Optical and electronic microscopy were employed to investigate on the crater shape, diameter and depth. SEM (Zeiss Crossbeam-540) was employed using 20 keV electron beam. A surface profiler (KLA Tencor-P 20) was used to furnish the surface profile with a depth resolution of 1 nm.

Table 1 reports some physical characteristics of the used targets useful to evaluate the laser spallation effects. The sound velocity is calculated at room temperature (20 °C).[20,21]

The sound velocity, calculated at room temperature in the bulk material, is related to the elastic Young's module Y and to the material density ρ, through the following relation[22]:

$$u = \sqrt{\frac{Y}{\rho}}. \tag{9}$$

3 | RESULTS

Typical IC and SiC spectra, relative to the laser irradiation of a thick target at 15° incidence angle in vacuum and to the ion emission along the normal to the target surface, are reported in Figure 2.

TABLE 1 Physical properties of different elements used as targets

Material	Density (g/cm^3)	Boiling point (°C)	Young's modulus (GPa)	Sound velocity (m/s)	Thermal conductivity (W/m K)	Tensile strength (MPa)	Hardness, Vickers (MPa)
PE	0.97	250	0.5	2,460	0.5	30	8.0
Al	2.7	2,450	70	6,420	235	130	200
Cu	8.96	2,595	130	4,760	400	250	350
Ge	5.32	2,237	135	5,400	60	135	8,012
Ag	10.5	2,210	83	3,650	430	180	251
Ta	16.6	5,425	186	3,400	57	760	870

Abbreviation: PE = polyethylene.

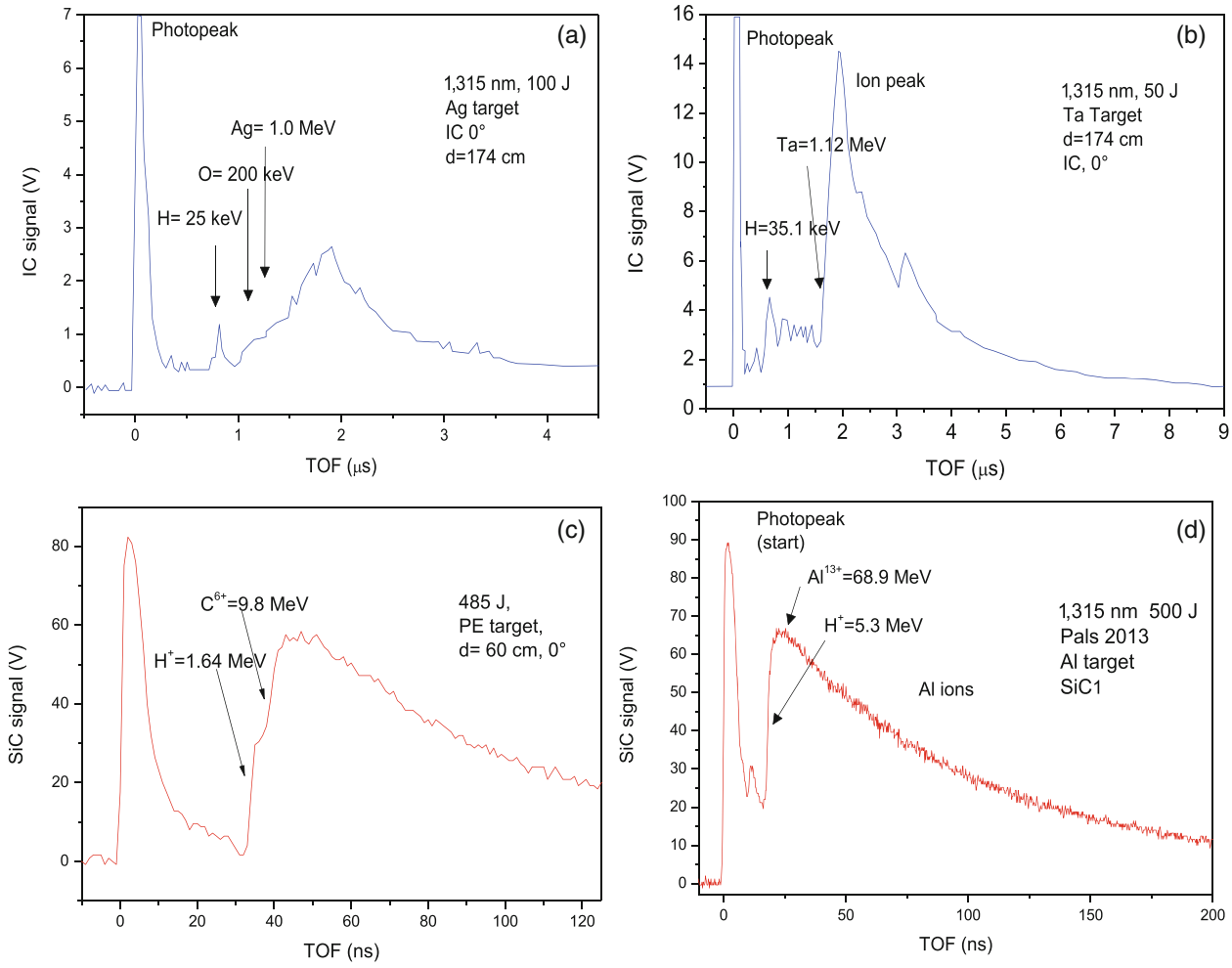

FIGURE 2 IC spectra for irradiation of Ag (a) and Ta (b) and SiC spectra for irradiation of PE (c) and Al (d)

In particular, Figure 2a shows the IC spectrum (d = 174 cm) of Ag ions obtained using a low laser pulse energy of 100 J in which the maximum proton energy is about 25 keV and the maximum ion energy for oxygen and silver are measured at 200 keV and 1.0 MeV, respectively. Assuming the proton energy to be representative of the ion energy acceleration per charge state, it means that the oxygen is ionized up to 8+ and the silver up to 40+. In such conditions, the evaluated maximum electron kinetic energy corresponds to a value above the ionization potential of Ag^{40+} and minor of the that of Ag^{41+}.

Using the NIST database[23] for ionization potentials is $I(Ag^{40+}) = 5.97$ keV and $I(Ag^{41+}) = 6.17$ keV, thus the maximum electron energy is of about 6 keV. Assuming the electron energy to have a Boltzmann distribution, its average energy

is about a fifth of its maximum value, that is, <E> = 6 keV/5 = 1.2 keV, at which corresponds to an average plasma temperature of about <kT> = (2/3)<E> = 0.8 keV.

Figure 2b shows the IC spectrum (d = 174 cm) of Ta ions obtained using a low laser pulse energy of 50 J in which the maximum proton energy is about 35.1 keV and the maximum ion energy for tantalum is 1.12 MeV. Assuming the proton energy to be representative of the ion energy acceleration per charge state, it means that the Ta ions are ionized up to 32+. Figure 2c shows the SiC spectrum (d = 60 cm) of H and C ions from PE target obtained using a high laser pulse energy of 485 J in which the maximum proton energy is about 1.64 MeV and the maximum carbon energy due to C6+ is about 9.8 MeV. Figure 2d shows the SiC spectrum (d = 60 cm) of Al target ions using a high laser pulse energy of 500 J in which the maximum proton energy is about 5.3 MeV and the maximum Al ion energy, due to Al^{13+}, is about 68.9 MeV.

Using the NIST ionization potential data book, in the case of high laser pulse energy in PE and Al, the electron energy is higher than 490 eV (ionization potential of C^{6+}) and 2.3 keV (ionization potential of Al^{13+}), respectively. Further plasma diagnostics occur for a better determination of the plasma electron temperature, such as the optical spectroscopy and the Langmuir probe analysis reported in the literature.[24,25]

The laser ablation yield, in terms of emitted mass per laser shot, grows with the pulse energy and is higher for materials with lower boiling points. Figure 3 shows an example of ablation yields in vacuum, for 1,350 nm wavelength and 300 ps pulse duration, for Ag, Cu and Ta targets versus the laser pulse energy. The crater depth and surface diameter are proportional to the laser pulse energy, according to the literature.[26] The removed mass is inversely proportional to the boiling point of the materials, in fact it is higher for silver, intermediate for copper and minor for tantalum, for which the boiling points are 2210 °C, 2595 °C and 5425 °C, respectively.[27]

The laser irradiations at different laser pulses have permitted to realize different shape and depth ablation craters, of which Figure 4 reports some optical photos. The figure reports the images of the laser ablation craters in Ag (front and back faces) (a), Cu (c), PE (d), Ta (e) and Ge (f) targets. In the case of Ag target, very ductile material, 2 mm thick, is reported also for the back-face, indicating that the plastic deformation due to the laser shockwave propagation at high intensity reach the back-face of the target. In the case of Ge-monocrystalline target—a very brittle material—it is possible to observe that the shockwave pressure destroys the crater formation and the Ge surface both at low than at high laser pulse energy and no regular crater is formed.

The crater details can be observed with attention using the SEM microscopy. Figure 5 reports a series of images for the Ag target as a function of the laser pulse energy. The craters are observed orthogonally to their aperture and laterally, at about 45°, showing that thermal effects of re-solidification of the melt influence the shape, the depth and the edges of each crater. The SEM images of Ag craters are referred to irradiation at 300 J (a, b), 150 J (c, d) and 75 J (e, f) laser energy. The three reported craters have a surface diameter of about 900 μm, 700 μm and 600 μm, respectively.

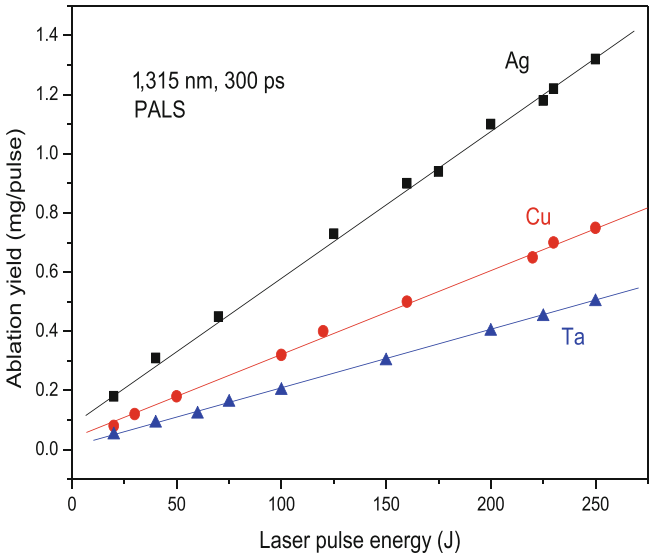

FIGURE 3 Ablation yield versus laser pulse energy for Ag, Cu and Ta targets

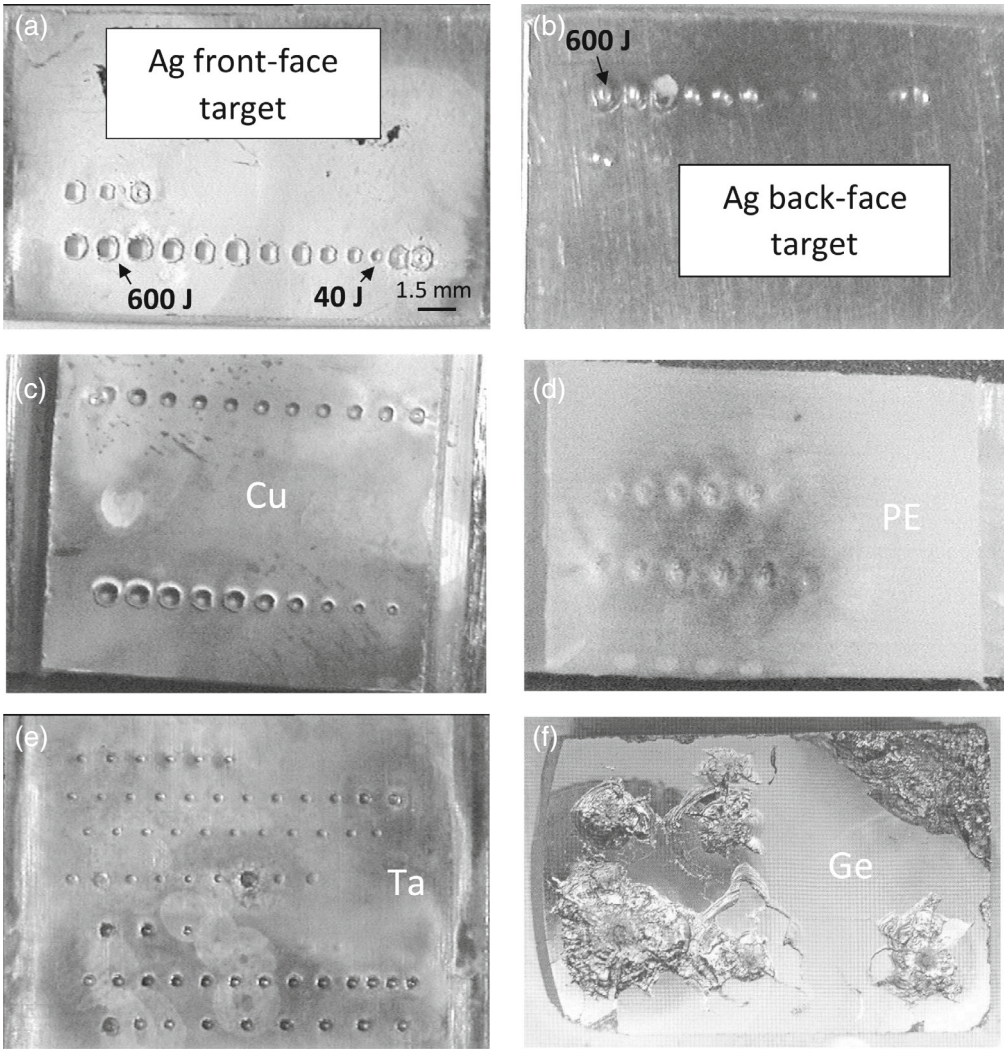

FIGURE 4 Images of the laser ablation craters in Ag (front and back faces) (a, b), Cu (c), PE (d), Ta (e) and Ge (f) targets

The intense laser shockwave produces plastic deformation in the back-face of the 2 mm Ag target, which is spherical shell shape, as evident from the SEM investigation reported in Figure 6. Such figure reports the back-face deformations produced by laser pulse of 400 J (a), 300 J (b), 200 J (c), 100 J (d), 75 J (e) and 40 J (f), respectively. At high laser intensity, it is possible to observe that the shockwave produces also back-face material emission.

Similar results were obtained for aluminium and copper targets, which maintain high thermal conductivity, similar to that of Ag. Figure 7 shows a crater in Cu produced by 200 J laser pulse and its protuberance on the back-face of the 2 mm target. Figure 7a shows the front side of the crater, Figure 7b shows the lateral side at about 45°, Figure 7c shows a zoom of the crater edge at high magnification and Figure 7d shows the spherical shell shape produced by the shockwave in the back-face of the Cu target.

In Ta target, 2 mm thick, the back-face does not show the presence of perturbation due to the shockwave; however, the bottom of the ablated crater, especially at high laser energies, shows conspicuous cracks caused by the high shockwave of laser light. Figure 8 shows four different craters in Ta produced by the high intensity laser at a pulse energy of 300 J (a), 200 J (b), 100 J (c) and 75 J (d). The inset of Figure 8a shows the crater depth profile acquired with the surface profiler along the crater diameter. The shockwave produces a crack in the crater bottom, which increases in size at higher pulse energy and disappears at lower pulse energy.

The crater deformations, cracks and back-face plastic deformations do not appear in the case of laser irradiation of PE, probably due to its low Young module, low sound velocity and high elasticity of the material that quickly dampens the pressure of the shockwave of the laser pulse. Figure 9 shows four different craters in PE produced by different laser pulse

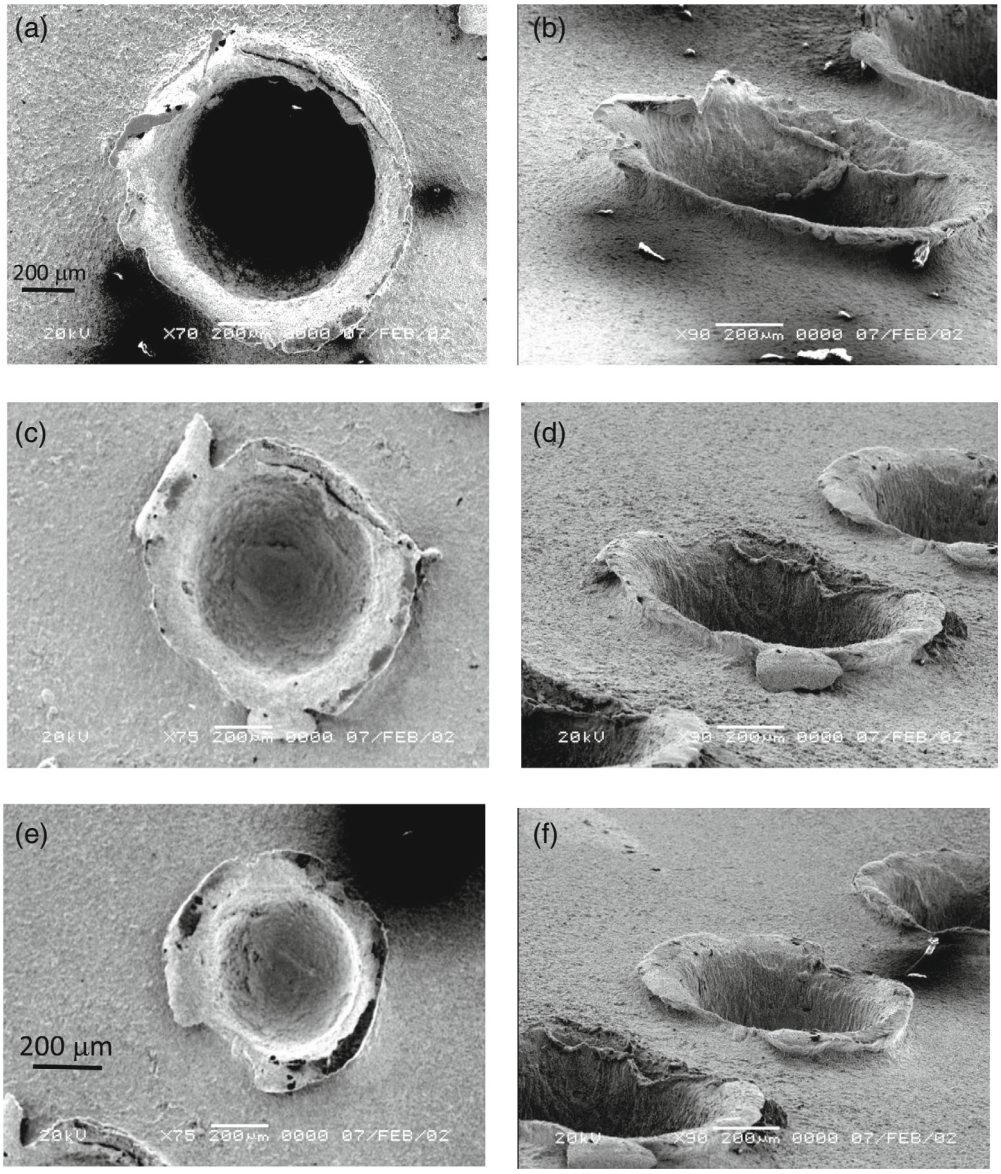

FIGURE 5 SEM images of Ag craters produced by 300 J (a, b), 150 J (c, d) and 75 J (e, f) laser energy

energy, at 300 J (a), 200 J (b), 100 J (c) and 75 J (d). In this last case, the plastic deformations induced by the shockwave are strongly damped and result less evident with respect to the metallic targets. However, at high laser energy, micrometric molecule clusters are present at the bottom of the crater, indicating that molecule scission, fusion and recombination occur.

4 | DISCUSSION

Because of the rapid energy deposition, thermal diffusion of energy away from the interaction zone in metals is limited to a few tens of microns. The heated material vaporizes, and the vapour rapidly achieves temperatures greater than several tens of thousands of degrees, whereupon electrons are ionized from the atoms and the vapour is transformed into a plasma. The plasma continues to strongly absorb the laser energy if its density is below the critical one.[28] If an overlay transparent to the laser light is pressed against the metal surface, the hydrodynamic expansion of the heated plasma in the confined region creates a high-amplitude short-duration pressure pulse and initiates a shock process, which compresses the walls of the crater.

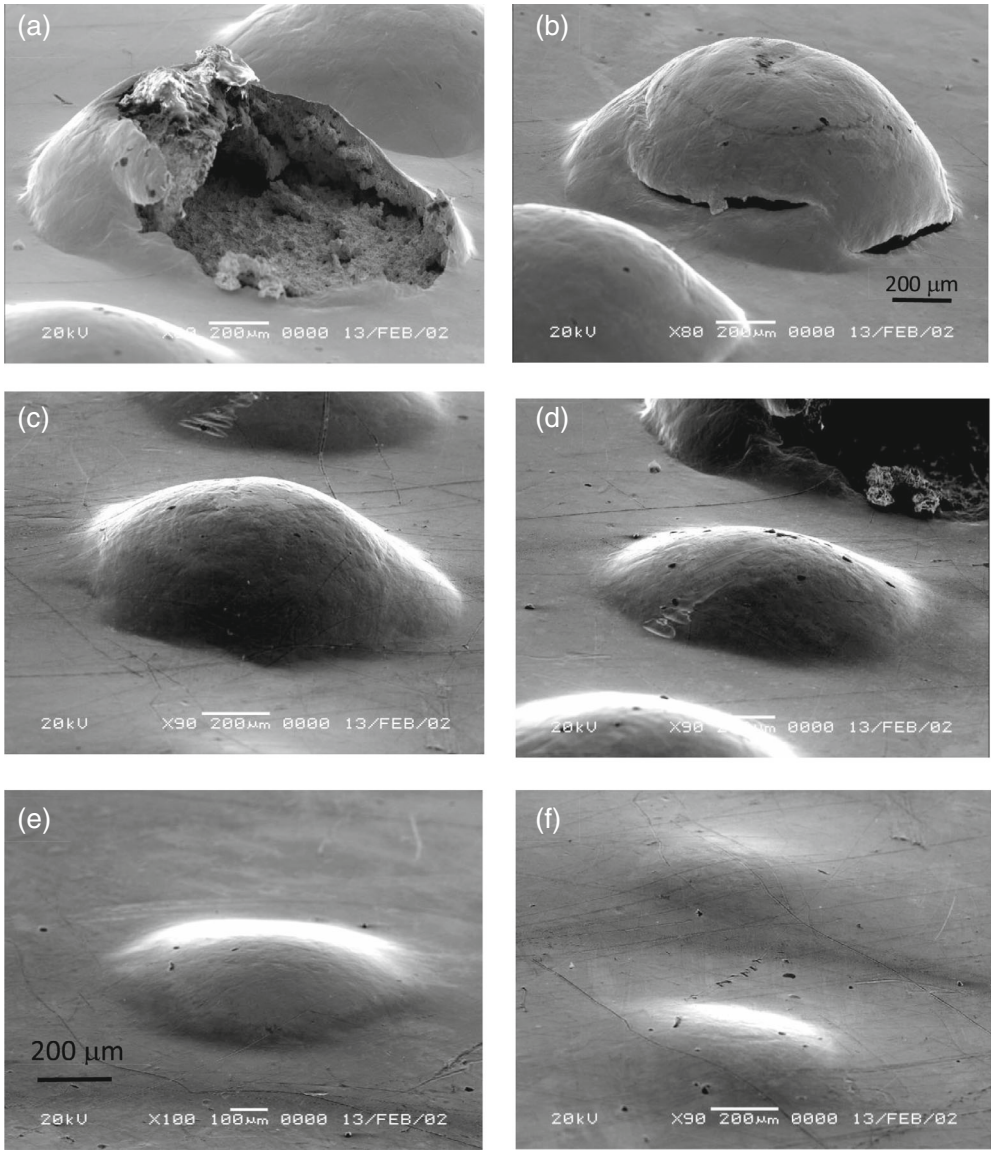

FIGURE 6 Ag back-face plastic deformation produced by laser pulse at 400 J (a), 300 J (b), 200 J (c), 100 J (d), 75 J (e) and 40 J (f), respectively

Taking in reference the case of Ag and Cu targets, in which the shockwave propagation produces deformation of the back-face of the 2 mm target, it is possible to evaluate some characteristics of the laser spallation effects. The shock theory focuses on point explosions, since laser-induced breakdown is characterized by an almost instantaneous release of a relatively large amount of energy in a very small volume.

For silver target, by SEM and surface profiler, investigations have been possible to evaluate the strain ε both longitudinally ($\Delta l/l$) than in volume ($\Delta V/V$). For example, by considering the effects induced by the high laser intensity obtained at 300 J laser pulse energy and observing the SEM images of Figures 5a and 6b, we can calculate a longitudinal strain:

$$\varepsilon = \frac{\Delta l}{l} = \frac{0.6\ mm}{2\ mm} = 0.3 = 30\%. \tag{10}$$

Considering the volume strain, it is:

$$\varepsilon = \frac{\Delta V}{V} = \frac{0.45\ mm^3}{1.27\ mm^3} = 0.35 = 35\%. \tag{11}$$

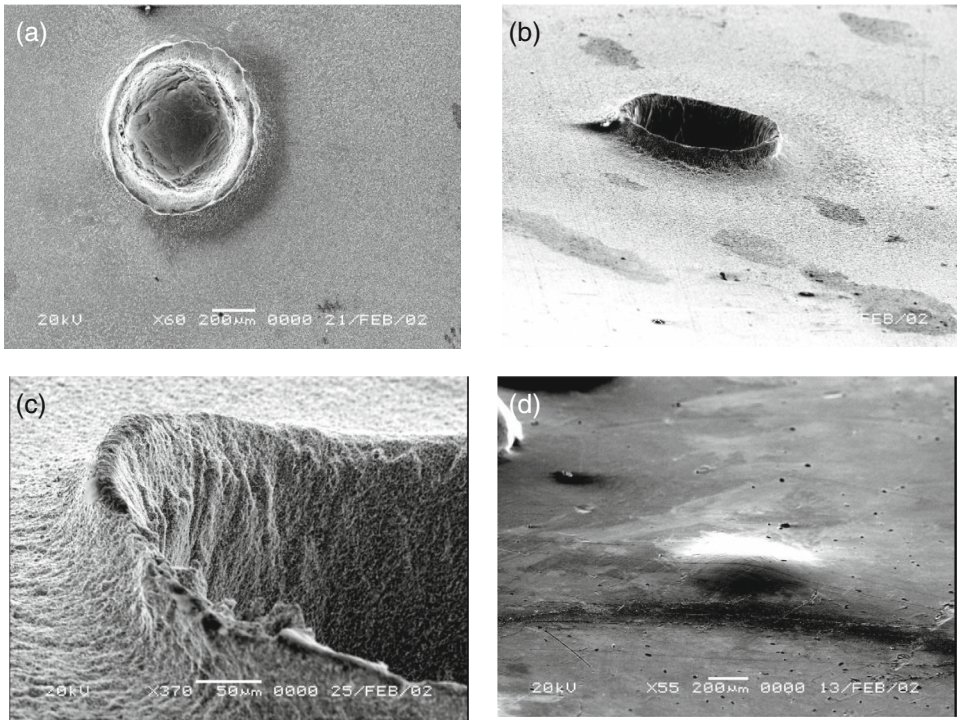

FIGURE 7 Ablation crater induced by 200 J laser pulse in 2 mm thick Cu target (a), crater edge (b, c) and spherical shell shape induced in the back-face of the target (d)

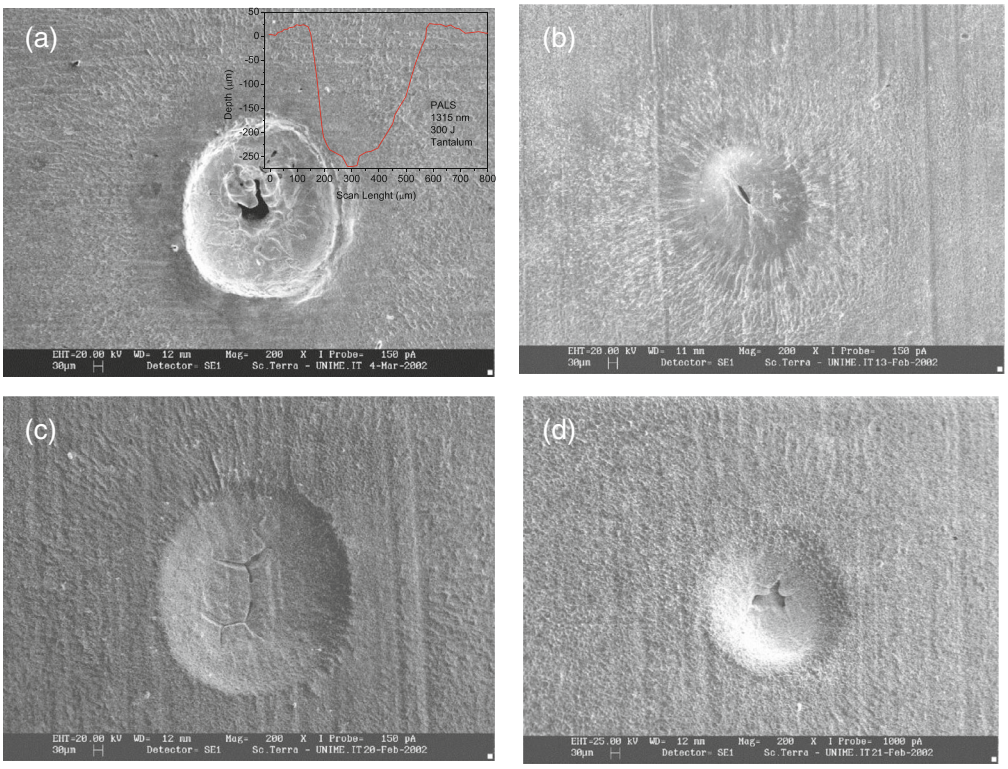

FIGURE 8 SEM image of Ta craters produced at a laser energy of 300 J (a), 200 J (b), 100 J (c) and 75 J (d). The inset of (a) shows the crater depth profile

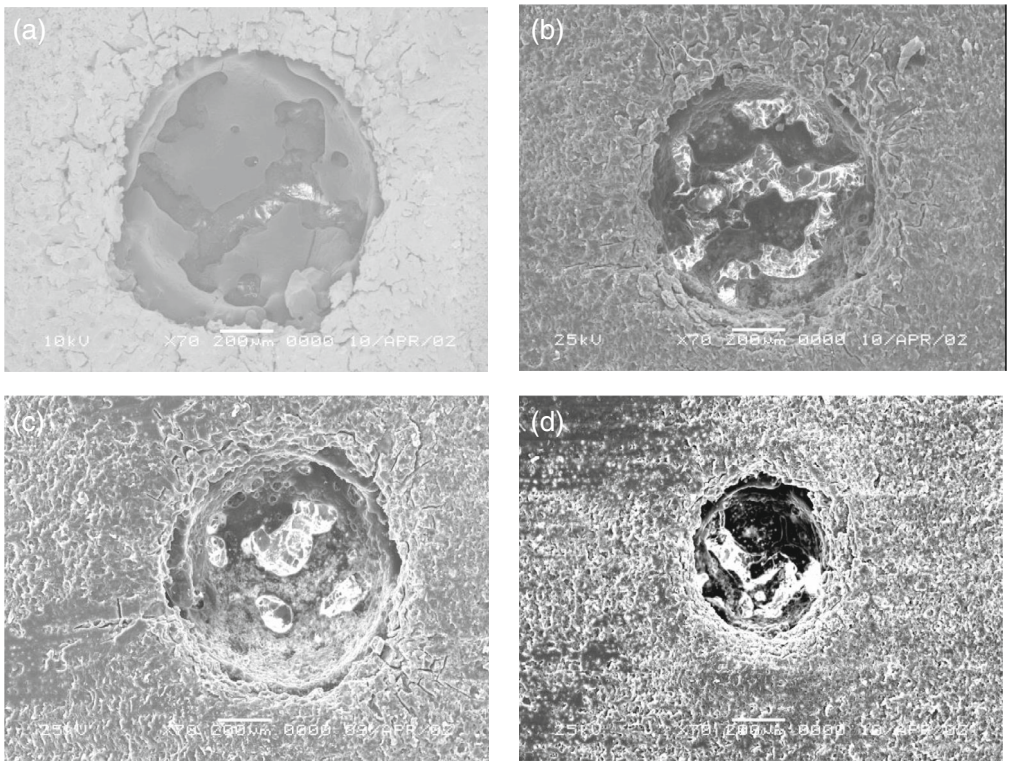

FIGURE 9 SEM image of PE craters produced at a laser energy of 300 J (a), 200 J (b), 100 J (c) and 75 J (d)

From Equation (4), the strain rate for the two cases assumes a value of:

$$\varepsilon_r \text{ (longitudinal)} = d\varepsilon/\mathrm{dt} = \frac{0.3}{300\ ps} = 10^9\ s^{-1} \tag{12}$$

$$\varepsilon_r \text{ (volume)} = d\varepsilon/\mathrm{dt} = \frac{0.35}{300\ ps} = 1.17 \times 10^9\ s^{-1} \tag{13}$$

Such values are comparable with the literature data.[1,4,22] The strain rate is not measurable for the targets that do not show significant plastic deformation measurable from the back-face surface, such as for PE and Ta.

In conditions of laser spot diameter (100 μm) minor of the target thickness (2 mm), the shockwave is constituted by spherical front-waves. The shockwave radius r_s calculable from Equation (5) for Ag target, relative to the 1 ns time after the laser pulse, that is, in near steady-state regime, assuming $E = 100$ J, $Y(\gamma) = 1$ and $\rho = 10.5$ g/cm^3, corresponds to:

$$r_s(t) = t^{2/5}(E/\rho)^{1/5}\ Y(\gamma) = (1\ ns)^{\frac{2}{5}}\left[100\ J/\left(10.5 \cdot 10^3 kg/m^3\right)\right]^{1/5} = 100\ \mu m \tag{14}$$

For PE and Ta, the targets used with the bigger mass density variation, the r_s value at 100 J pulse energy corresponds to 159 μm and 90 μm, respectively. Such radius is comparable with the used diameter of the laser spot focus on the target surface and is smaller to the target thickness. It slowly depends on the time and on the target density, but is strongly dependent on the laser pulse energy.

The shockwave expansion velocity in Ag is supersonic and, using Equation (6), for 1 ns time after the laser shot is:

$$v_s(t) = \frac{dr_s}{dt} = \frac{2}{5}\ t^{-3/5}(E/\rho)^{1/5}\ Y(\gamma) = \frac{2}{5}(1\ ns)^{-\frac{3}{5}}\ \left[100\ J/\left(10.5 \cdot 10^3 kg/m^3\right)\right]^{1/5} = 3.95 \cdot 10^4 \frac{m}{s} \tag{15}$$

Of course, this velocity is smaller to the maximum Ag ion velocity in vacuum corresponding to the maximum kinetic energy conferred by Coulomb acceleration of 1 MeV, which is 1.3×10^6 m/s (see TOF spectrum in Figure 2a).

In the approximation that $Y(\gamma) = 1$, its value in PE and Ta corresponds to 0.64×10^4 m/s and 3.61×10^4 m/s, respectively.

Such velocity values are comparable with those reported in the literature.[29]

Thus, in Ag, the shockwave Mach number, calculable from Equation (7), assuming the sound velocity at room temperature $\underline{u} = 3650$ m/s (see Table 1) is:

$$M_s(t) = \frac{v_s(t)}{u\,(T)} = \frac{3.95 \cdot 10^4\ m/s}{3650\ m/s} = 10.82 \tag{16}$$

By considering the sound velocities reported in Table 1, the Mach number for PE and Ta becomes 2.60 and 10.62, respectively.

Due to the high propagation velocity of the shockwave, the request time to transmit it to the back-face of the target, 2 mm distant, where it is reflected towards the surface, is calculable. For Ag, it corresponds to about 50 ns, while for PE and Ta targets it is about 588 ns and 55 ns, respectively. Such times are very higher than the laser pulse duration of 300 ps, in fact they are about a factor 167, 1960 and 183 times higher for Ag, PE and Ta, respectively. During this time, the shockwave may be reduced in intensity due to damping, especially in low hardness materials such as PE, which is inner compressed and increased in density. Consequently, its back-face is not plastic deformed. In Ta, the back-face is not deformed, probably due to its high hardness and tensile strength and to the shockwave decreasing with the distance and time.

Finally, the pressure jump, Δp, across the shockwave in Ag target can be calculated from Equation (8), assuming the shockwave radius corresponding to that of 1 ns and the parameter $Y^5(\gamma)/(\gamma+1) = 0.25$, as reported in the literature[15,30]:

$$\Delta p = \frac{8}{25}\left(\frac{E}{r_s^3}\right)\left[Y^5(\gamma)/(\gamma+1)\right] = 0.32 \cdot \left[100\frac{J}{\left(100 \cdot 10^{-6}\right)^3 m^3}\right] \cdot 0.25 = 8 \times 10^{12}\ Pa \tag{17}$$

A value much higher than the tensile strength of any material, but it is calculated very near to the laser shot.

Such value is comparable with literature data and can be given in energy density units (J/cm^3).[28]

At high laser intensity, above 10^{15} W/cm^2, literature reports, on aluminium and other metallic targets such as that used in this experiment, pressure values above 1 TPa,[31] 3 TPa[32] and 4 TPa,[33] and others, all comparable with the value calculated through the theoretical prediction given by Equation (17).

The value of calculated r_s, v_s, M and Δp, after 10 ns from the laser shot, for the different used targets, are reported in Table 2.

Thus, r_s and v_s are inversely proportional to the target density, while the pressure enhances with the density, as reported in Figure 10.

Certainly the pressure jump, Δp, across the shockwave in Ag target can be calculated from Equation (8), assuming the shockwave radius of 2 mm, corresponding to the target thickness, and the parameter $Y^5(\gamma)/(\gamma+1) = 0.25$, as reported in the literature[15,30]:

$$\Delta p = \frac{8}{25}\left(\frac{E}{r_s^3}\right)\left[Y^5(\gamma)/(\gamma+1)\right] = 0.32 \cdot \left[100\frac{J}{\left(2 \cdot 10^{-3}\right)^3 m^3}\right] \cdot 0.25 = 1.0\ GPa. \tag{18}$$

TABLE 2 Evaluation of r_s, v_s, M and Δp after 10 ns from the laser shot for all investigated targets

Target	r_s (μm) (10 ns, 100 J)	v_s ($\times 10^4$ m/s)	M	Δp ($\times 10^{12}$ Pa)
PE	159	0.637	2.59	1.98
Al	130	5.19	8.08	3.65
Cu	102	4.08	8.57	7.50
Ge	113	4.53	8.39	5.52
Ag	99	3.95	10.82	8.23
Ta	90	3.61	10.62	10.98

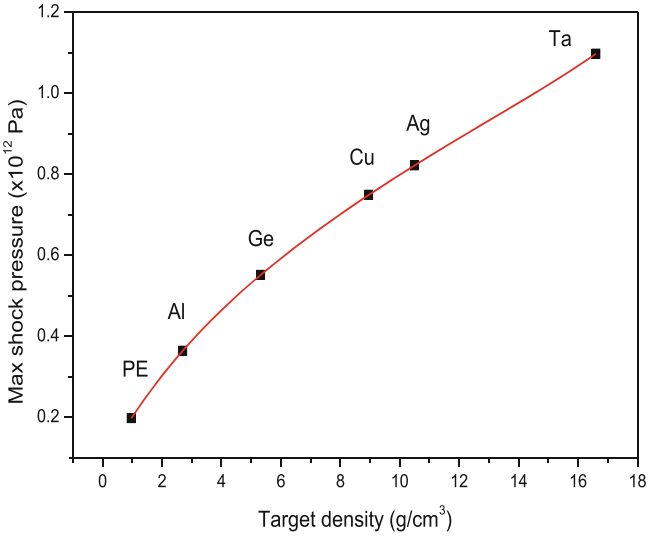

FIGURE 10 Calculated max shock pressure versus the target density

TABLE 3 Observed plastic deformations or no deformations in the irradiated targets for the laser condition used

Target	Δ*P* (2 mm distance)	Compressive strength (MPa)	Plastic deformation
PE	1 GPa	40	No (damping)
Al	1 GPa	280	Yes
Cu	1 GPa	330	Yes
Ge	1 GPa	2,400	No (cracks)
Ag	1 GPa	300	Yes
Ta	1 GPa	1,060	No (cracks)

A value much higher than the compressive strength of silver of 300 MPa.[34]

This shockwave pressure is higher that the compressive strength of many used materials but minor of that of Ge and Ta, materials in which we have not shown deformation after the laser shot.

Table 3 shows the cases in which using the laser condition parameters of 100 J pulse energy on a laser spot of 7.85×10^{-5} cm^2, and 2 mm target thickness, the shockwave produces plastic deformations or no deformation.

The ΔP calculated values are not corrected for the attenuation of the shockwave with the distance ad time, in fact the compressed matter produces damping and determines a pressure decreasing with distance and time.

The laser-induced high shock waves can produce hardening across the entire region of the laser-irradiated area, as reported in the literature.[5]

In monocrystalline Ge, these high pressures induce rupture and flaking of the target surface layers as shown in Figure 4f. In soft PE and Al target, the pressure is strongly reduced by damping with the distance due to its inner compression effect. In Ta, no plastic deformation was observed, in agreement with the data reported in Table 3 but only cracks in the crater bottom.

The hardness gradient and the shocked surface of laser-irradiated targets indicate that a surface residual stress after laser shocking is present. The residual stresses are compressive and seem relatively uniform across the radius of the laser-shocked region.

5 | CONCLUSIONS

The high intensity sub-ns lasers induce high shockwaves in the target, which, at supersonic velocity, cross the target thickness and are reflected by the back-face returning to the surface. The target material is subjected to a strong pressure

variation that may determine the rupture of the target, such as occurring for Ge, the formation of spherical shell in the back-face, 2 mm distant from the front-face, as occurring for Ag, Cu and Al, and the formation of craters in which the confinement of the plasma in the bottom material my determine ruptures and cracks, as occurring in Ta targets. In polymers, instead, the low propagation velocity determines a pressure damping and absence of plastic deformation in the back-face at 2 mm distance, as occurring in high-density PE. However, molecular scission, fusion and nucleation are observed in this case.

The pressure wave travels at supersonic speed and very high Mach numbers greater than 10 can be evaluated for Ag and Ta, values around 8 for Ge, Cu and Al and a value of about 2.5 for high-density PE.

The pressure value generally is higher than the tensile strength of the material, but in elastic targets, such as PE, it does not induce macroscopic ruptures due to its strong decay with the distance and time.

This pressure, of the order of GPa, depends strongly on the laser intensity and less on the target properties.

The laser-induced shock wave can produce hardening across the entire region of the laser-irradiated area, according to the literature. Thus, multiple laser shots can produce a progressive increase in hardness of many materials. The shockwave can be employed to improve adhesion between different interfaces, to clean surfaces, to induce compression and density increment and to produce molecular clustering.

Measurements of the ablation yield and ion acceleration induced by the non-equilibrium plasma are also presented, in order to characterize the plasma produced by the 300 J and 300 ps laser shot by different types of targets.

Further measurements are in progress on the residual stresses in different material targets, which are compressive and seem relatively uniform across the radius of the laser-shocked region.

ACKNOWLEDGMENTS

The authors thank the LaserLab-Europe for the useful support given and all the staff of the PALS Laboratory. Open Access Funding provided by Universita degli Studi di Messina within the CRUI-CARE Agreement.

DATA AVAILABILITY STATEMENT

Research data are not shared.

REFERENCES

[1] H. Ehsani, J. D. Boyd, J. Wang, M. E. Grady, *Appl. Mech. Rev.* **2021**, *73*(3), 030802.
[2] S. Eliezer, I. Gilath, T. Bar-Noy, *J. Appl. Phys.* **1990**, *67*, 715.
[3] B. Rethfeld, D. S. Ivanov, M. E. Garcia, S. I. Anisimov, *J. Phys. D: Appl. Phys.* **2017**, *50*, 193001.
[4] Y. Fan, Y. Wang, S. Vukelic, Y. L. Yao, *J. Appl. Phys.* **2005**, *98*, 104904.
[5] A. H. Clauer, J. H. Holbrook, B. P. Fairand, in Shock Waves and High-Strain-Rate Phenomena in Metals (Eds: M. A. Meyers, L. E. Murr), Plenum Publishing Corporation, New York **1981**, Ch.38.
[6] A. M. Mostafa, M. F. Hameed, S. S. Obayya, *J. King Saud Univ. – Sci.* **2019**, *31*, 472.
[7] S. Eliezer Ed., The Interaction of High-Power Lasers with Plasmas, IOP Publishing, Bristol, UK **2002**.
[8] D. D. Mallick, J. Parker, J. W. Wilkerson, K. T. Ramesh, *J. Dyn. Behav. Mater.* **2020**, *6*, 268.
[9] D. J. Griffiths, Introduction to Electrodynamics, 3rd ed., Addison-Wesley, Boston, MA **2012**.
[10] Y. Wang, C. Liu, C. Li, *Results Phys.* **2021**, *22*, 103920.
[11] D. C. Swift, T. E. Tierney, R. A. Kopp, J. T. Gammel, *Phys. Rev. E* **2004**, *69*, 036406.
[12] C. Zhou, Y. Bai, Z. Li, Y. Ding, H. Sun, Y. Tian, *Eur. Phys. J. Appl. Phys.* **2020**, *91*, 10801.
[13] T. De Rességuier, J. P. Cuq-Lelandais, M. Boustie, E. Lescoute, L. Berthe, in Wave Propagation in Materials for Modern Applications (Ed: A. Petrin), InTech, Croatia **2010**, p. 526. https://www.researchgate.net/publication/221906719.
[14] G. Sinibaldi, A. Occhicone, F. A. Pereira, D. Caprini, L. Marino, F. Michelotti, C. M. Casciola, *Phys. Fluids* **2019**, *31*, 103302.
[15] N. A. Lammers, *Master Thesis*, Eindhoven University of Technology, **2022**.
[16] FZU, PALS - Prague Asterix Laser System, 2022.
[17] M. Cutroneo, P. Musumeci, M. Zimbone, L. Torrisi, F. La Via, D. Margarone, A. Velyhan, J. Ullschmied, L. Calcagno, *J. Mater. Res.* **2012**, *28*(1), 87.
[18] L. Torrisi, G. Foti, L. Giuffrida, D. Puglisi, J. Wolowski, J. Badziak, P. Parys, M. Rosinski, D. Margarone, J. Krasa, A. Velyhan, J. Ullschmied, *J. Appl. Phys.* **2009**, *105*, 123304.
[19] J. Ziegler, M. Ziegler, J. Biersack, *Nucl. Instrum. Methods Phys. Res. Sect. B* **2008**, *268*, 1818.
[20] Sensagent, Speeds of sound of the elements data page, 2022: speeds of sound of the elements data page: definition of speeds of sound of the elements data page and synonyms of speeds of sound of the elements data page (English) (sensagent.com).
[21] Evident, Material Sound Velocities, olympus-ims.com, 2022.
[22] K. Langer, S. Olson, R. Brockman, W. Braisted, T. Spradlin, M. E. Fitzpatrick, *J. Eng.* **2015**, *2015*(13), 150.
[23] NIST, Atomic Spectra Database Ionization Energies Data, 2022.

[24] L. Torrisi, A. Borrielli, D. Margarone, F. Caridi, A. M. Mezzasalma, *Eur. Phys. J. D* **2008**, *54*(2), 343.
[25] L. Torrisi, M. Cutroneo, S. Cavallaro, *IEEE Trans. Plasma Sci.* **2014**, *42*(3), 799.
[26] L. Torrisi, S. Gammino, A. M. Mezzasalma, A. M. Visco, J. Badziak, P. Parys, J. Wolowski, E. Woryna, J. Krasa, L. Laska, M. Pfeifer, K. Rohlena, F. P. Boody, *Appl. Surf. Sci.* **2004**, *227*, 164.
[27] L. Torrisi, A. Borrielli, D. Margarone, *Nucl. Instrum. Methods Phys. Res. Sect. B* **2007**, *255*, 373.
[28] D. Giulietti, L. A. Gizzi, *Riv. Nuovo Cim.* **1998**, *21*, 1.
[29] R. J. Trainor, N. C. Holmes, R. A. Anderson, presented at Proc. American Physical Society, Topical Conf. on Shockwave in Condensed Matter, Menlo Park, CA, June 22–24, 1981.UNT Digital Library, pp. 2–10.
[30] Z. Henis, S. Eliezer, E. Raicher, *Laser Part. Beams* **2019**, *37*, 268.
[31] N. C. Holmes, R. J. Trainor, R. M. More, R. A. Anderson, presented at Proc. Conf. 1979 IEEE/QSA Conf. on Laser Engineering and Applications Washington, DC, May 30–June 1, 1979, Materials Processing, Biomedical and Novel Applications, p. 1D.
[32] F. Cottet, J. P. Romain, R. Fabbro, B. Faral, *Phys. Rev. Lett.* **1984**, *52*(21), 1884.
[33] R. J. Trainor, N. C. Holmes, R. M. More, presented at Proc. VIIth Intern. AIRAPT Conf., Le Creusot, France, July 30–August 3, 1979, 1980, pp. 965–967.
[34] AZO Materials, Properties: Silver - Applications and Properties of Silver, 2022, azom.com.

How to cite this article: L. Torrisi, A. Torrisi, *Contributions to Plasma Physics* **2023**, *63*(1), e202200092. https://doi.org/10.1002/ctpp.202200092